International Tables for X-ray Crystallography (1959). Vol. II. Birmingham: Kynoch Press.
International Tables for X-ray Crystallography (1974). Vol. IV. Birmingham: Kynoch Press.
KARLSSON, R. (1976). *Acta Cryst.* B**32**, 2609–2614.
PARTHASARATHY, R. (1962). *Acta Cryst.* **15**, 41–46.
PENZIEN, K. & SCHMIDT, G. M. J. (1969). *Angew. Chem. Int. Ed. Engl.* **8**, 608–609.
RABINOVICH, D. & HOPE, H. (1975). *Acta Cryst.* A**31**, S128.
RABINOVICH, D. & SHAKKED, Z. (1974). *Acta Cryst.* B**30**, 2829–2834.
RABINOVICH, D. & SHAKKED, Z. (1975). *Acta Cryst.* B**31**, 819–825.
SHERWOOD, J. N. & THOMSON, S. T. (1960). *J. Sci. Instrum.* **37**, 242–245.
VOS, A. (1975). In *Anomalous Scattering*, edited by S. RAMASESHAN & S. C. ABRAHAMS, pp. 307–339. Copenhagen: Munksgaard.

Acta Cryst. (1980). A**36**, 678–682

Oxidation Reactions in Natural Fe–Ti Oxide Spinels

BY R. FROST*

Department of Geology and Mineralogy, University of Oxford, Parks Road, Oxford OX1 3PH, England

AND P. L. GAI

Department of Metallurgy and Science of Materials, University of Oxford, Parks Road, Oxford OX1 3PH, England

(*Received* 21 *January* 1980; *accepted* 18 *February* 1980)

Abstract

Defects and oxidation reactions in naturally occurring Fe–Ti oxide spinels have been investigated by a combination of *in situ* environmental-cell high-voltage electron microscopy (HVEM) and high-resolution lattice-imaging electron microscopy (HREM) methods. The experiments conducted on the magnetite–ulvöspinel (Fe_3O_4–Fe_2TiO_4) system show that partial oxidation to cation-deficient cubic spinels sometimes occurs before the oxidation of the system to the rhombohedral hematite–ilmenite oxides (Fe_2O_3–$FeTiO_3$).

Introduction

The possible compositions of naturally occurring mineral spinels have been reviewed by Lindsley (1976). Industrial applications have caused considerable interest in Fe–Ti oxides in recent years. However, experimental work on these systems is limited at temperatures below ~1273 K and is mostly done on simple synthetic minerals. It is, therefore, felt that with natural minerals as starting materials a clearer understanding of oxidation reactions in specific environments may be obtained. The development of an environmental cell in the HVEM (Swann & Tighe, 1971) has allowed such reactions to be observed directly under controlled atmospheres. Flowers, Tighe & Swann (1974) for example were able to perform controlled reduction experiments on hematite–magnetite and Thoeni, Gai & Hirsch (1977) on oxide catalyst systems. The present experiments were designed to observe oxidation reactions in complex magnetite–ulvöspinel systems.

Experimental

Samples from an ore vein in a ferrogabbro from a middle zone of Skaergaard intrusion (East Greenland) rich in these minerals were used. They were cut with a diamond saw, polished, and thinned with an ion beam. The sample compositions were determined with an electron-microscope microanalyser and crystal structures were determined by X-ray and electron diffracton. For HREM work, a recently installed JEOL JEM 200CX electron microscope fitted with a LaB_6 gun and operating at 200 kV was used. The performance characteristics of the JEM 200CX electron microscope have been described by Boyes *et al.* (1980). Thinned samples were examined at magnifications up to a million and micrographs were recorded between about −700 and −900 A defocus in steps of ~90 Å with an objective aperture to include diffracted beams out to about 0·6 $Å^{-1}$. Many-beam-contrast calculations were carried out where necessary to interpret the images. The oxidation reactions on the samples were conducted in an environmental cell fitted to an

* Now at: British Steel Corporation, Middlesbrough, England.

0567-7394/80/040678-05$01.00

AEI-EM7 HVEM operating at 1 MeV, at oxygen pressures of ~ $1{\cdot}3 \times 10^4$ Pa from room temperature (r.t.) to ~1098 K. Platinum strip heaters were used in the cell and were calibrated by a Pt–13% Pt–Rh thermocouple for various gas pressures and environments (Gai, 1980).

Results and discussion

Magnetite is cubic, space group $Fd3m$, with $a = 8{\cdot}396$ Å. There are 24 Fe and 32 O atoms per unit cell. On this basis the calculated diffraction patterns of magnetite from [010] and [110] zones from a relatively thin crystal are shown in Fig. 1(*a*) and (*b*), scaled to kinematical beam intensities. The reflections of the type $g = 100$ and 200 *etc.* are absent due to the space-group limitations. However, in some experiments $g = 200$-type reflections were observed near to [110] orientations and their presence may be attributed to double-diffraction effects (Smith, 1978). Ulvöspinel, which is once again cubic with space group $Fd3m$ and $a = 8{\cdot}536$ Å, has 16 Fe and 8 Ti metal atoms per unit cell. The Ti atoms occupy random positions within the octahedral sites and are placed so as to preserve the space-group symmetry. The extinction distances (E_g) for some of the reflections for example are calculated [with relativistic corrections and scattering factors described in Smith & Burge (1962)]:

(*a*) for magnetite, E_g's are, for $g(040) = 640$, $g(220) = 1220$, $g(111) = 2827$, $g(440) = 513$, $g(113) = 820$ Å and so on.

(*b*) for ulvöspinel, they are, for $g(040) = 717$, $g(220) = 1198$, $g(111) = 2505$, $g(440) = 565$, $g(113) = 883$ Å and so on.

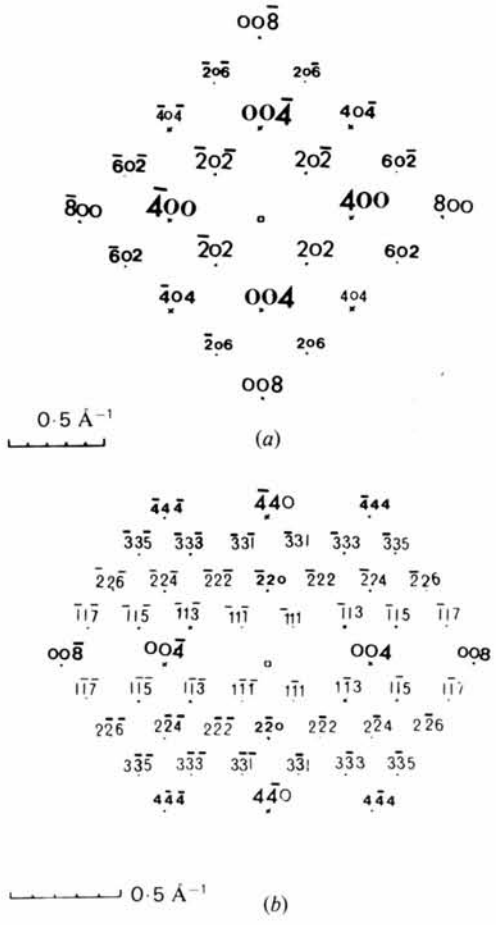

Fig. 1. Calculated diffraction patterns for magnetite scaled to kinematical beam intensities. (*a*) [010] zone, (*b*) [110] zone.

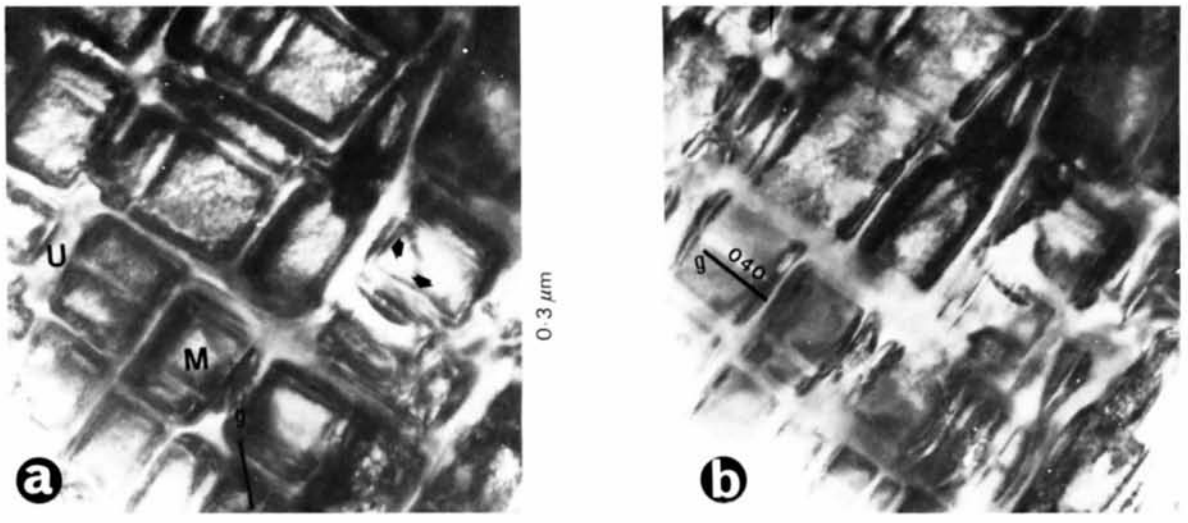

Fig. 2. Cubes of magnetite and lamellae of ulvöspinel [in (001) section] represented by *M* and *U* respectively showing two sets of dislocations (arrowed) at the boundaries. (*a*) $g = 220$ reflection. (*b*) One set is absent in $g = 040$.

(*a*)

(*b*)

Fig. 3. High-resolution lattice images of the spinel magnetite recorded at 200 kV. (*a*) (100) section, (*b*) (110) section. The insets show computed images of the structures.

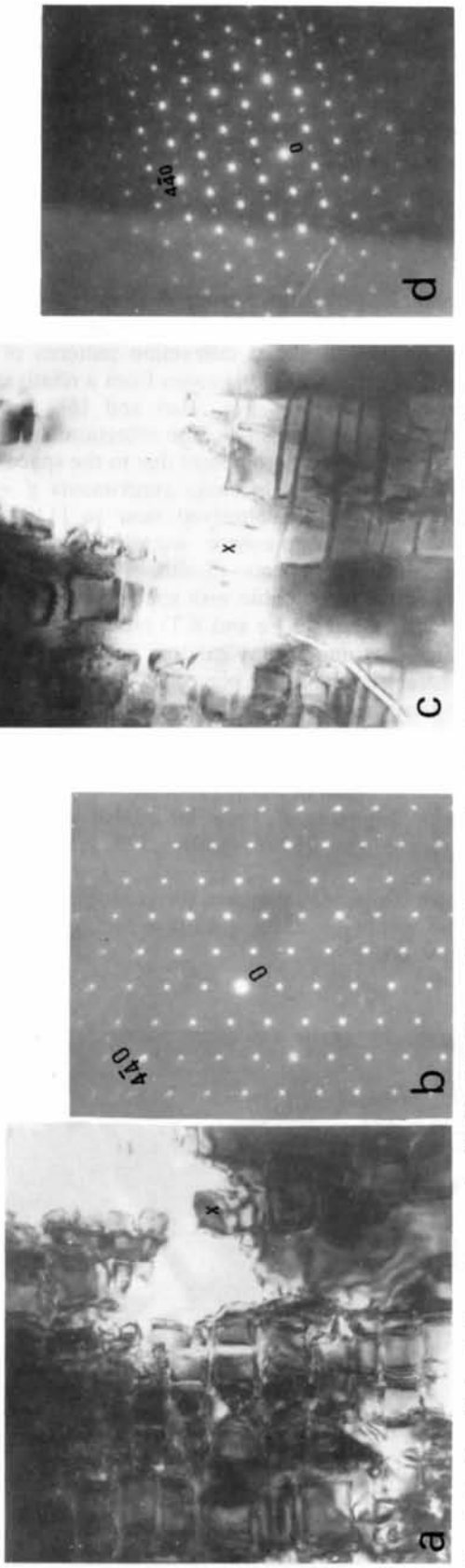

Fig. 4. Partial oxidation in the environmental cell of the HVEM at ~753 K in oxygen (1 MeV). (*a*) Image before oxidation, (*b*) [110] diffraction pattern before oxidation, (*c*) image after oxidation, (*d*) diffraction pattern showing superlattice spots.

The micrographs of the mineral show cubes of magnetite and lamellae of ulvöspinel, their composition determined by EMMA and electron microprobe. Fig. 2(*a*) shows an example taken in $g = 220$ reflection where regions of magnetite and ulvöspinel are shown by *M* and *U* respectively. The micrographs also revealed two sets of dislocations (indicated by the arrows) at the boundaries of the two phases. One set is absent in $g = 040$ reflection as shown in Fig. 2(*b*). Analysis of the defect contrast in various reflections by tilting the specimen in the electron microscope and comparing with contrast calculations for various models of displacement vectors showed the dislocations to be of edge character with Burgers vector $\mathbf{b} = (a/2)\,[101]$ type. During the subsolidus exsolution, these defects are presumably generated to accommodate the change at magnetite–ulvöspinel phase boundaries.

The high-resolution micrographs taken at 200 kV reveal the structures of the spinel lattice of a magnetite region in [100] and [110] zones as shown in Figs. 3(*a*) and (*b*) respectively. The insets show computed images of the structure.

The samples of the mineral were oxidized in the HVEM in pure oxygen. Temperatures below 673 K did not significantly affect the specimens oxidized for periods of time of up to ~15 min. However, the samples heated in oxygen at 673–873 K exhibited superlattice spots in the diffraction pattern and detailed analysis of the samples and diffraction patterns in various orientations showed them to correspond to a cation-deficient cubic spinel phase. Figs. 4(*a*) and (*b*), for example, show the sample before oxidation near to the [110] zone and (*c*) and (*d*) after oxidation. The lattice parameter deduced from the diffraction patterns is $a \simeq 8{\cdot}3$ Å and is close to the cubic γ-Fe_2O_3 phase. At temperatures >873 K, however, with fast oxidation times of several minutes, regions in the specimens furnished diffraction patterns in several areas typical of rhombohedral (or pseudo-hexagonal) hematite–ilmenite structures as shown in the diffraction pattern in Fig. 5 for a sample at ~1073 K. Hematite and ilmenite have almost similar lattice parameters; for hematite, $a \simeq 5{\cdot}04$, $c \simeq 13{\cdot}8$ Å and for ilmenite, $a \simeq 5{\cdot}082$, $c \simeq$

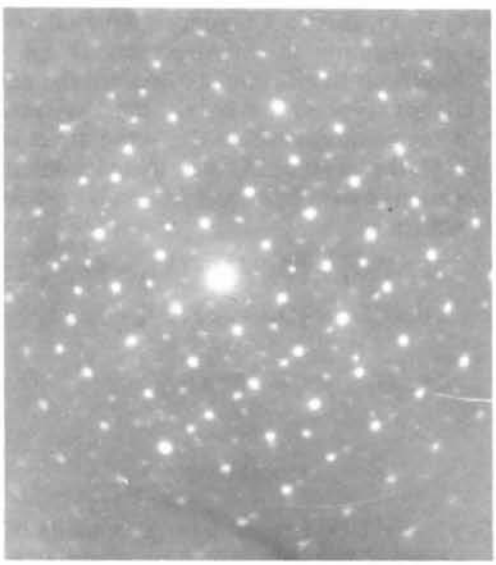

Fig. 5. Diffraction pattern from the specimens oxidized at ~1073 K, typical of rhombohedral (pseudo-hexagonal) hematite–ilmenite structures.

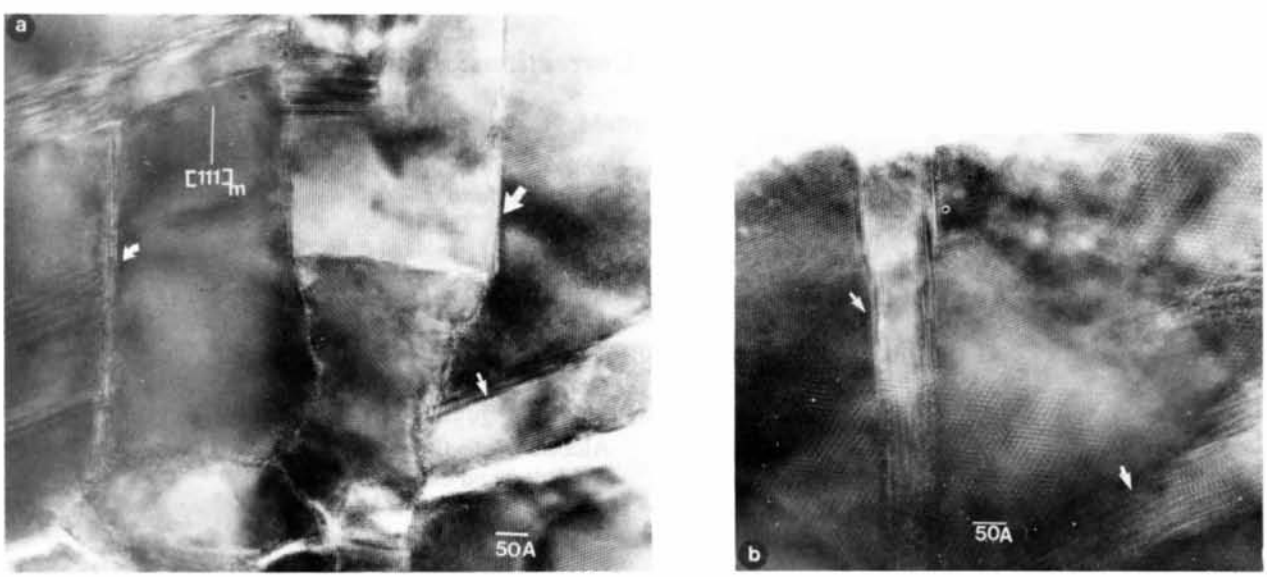

Fig. 6. (*a* and *b*) Lattice images (at 200 kV) from samples oxidized at ~1073 K, showing microstructures of various interfaces of hematite or ilmenite lamellae (arrowed) with a growth habit of $(111)_m \parallel (0001)_{h/i}$.

14·026 Å. Analysis of the lattice images from these areas showed hematite/ilmenite (*h/i*) lamellae about 30–300 Å wide in magnetite–ulvöspinel with a growth habit of $(111)_m \parallel (0001)_{h/i}$ as shown in the examples of Figs. 6(*a*) and (*b*), the direction of growth being similar to that observed in the natural ilmenite samples. However, in some samples during slow oxidation experiments conducted for several hours at lower temperatures, it was possible to observe the growth along $[100]_m$ indicating the replacement of the ulvöspinel phase (Frost, 1979).

In the oxidation reactions described it seems likely that both Fe_3O_4 and Fe_2TiO_4 undergo partial oxidation. The close similarity in the structures of the phases makes it difficult to differentiate between the nature of the oxidation process governing the two phases at different temperatures within the small areas (<200–300 Å) of the crystals. Under these conditions the incorporation of oxygen in magnetite–ulvöspinel can be simply written as

$$3Fe_2TiO_4 + \tfrac{1}{2}O_2 \rightarrow 3FeTiO_3 + Fe_3O_4,$$

$$2Fe_2TiO_4 + \tfrac{1}{2}O_2 \rightarrow 2FeTiO_3 + Fe_2O_3$$

and

$$2Fe_3O_4 + \tfrac{1}{2}O_2 \rightarrow 3Fe_2O_3.$$

Conclusions

The Fe_3O_4–Fe_2TiO_4 natural mineral consists of cubes of magnetite and lamellae of ulvöspinel with two sets of edge dislocations at the boundaries of the two phases generated during the subsolidus exsolution. The direct observations of oxidation experiments on these minerals have revealed that a cation-deficient cubic intermediate phase may sometimes occur in the oxidation of magnetite–ulvöspinel to rhombohedral hematite–ilmenite. When the oxidation temperature is >873 K, hematite/ilmenite lamellae grow into the magnetite–ulvöspinel with the $(111)_m \parallel (0001)_{h/i}$ habit.

We thank Professor Sir Peter Hirsch, FRS, for the provision of laboratory facilities, Professor E. A. Vincent of the Department of Geology & Mineralogy, Oxford, for helpful suggestions, NERC and SRC for financial support and Dr A. J. Skarnulis for the provision of interactive computing facilities.

References

BOYES, E. D., WATANABE, E., SKARNULIS, A. J., HUTCHISON, J. L., GAI, P. L., JENKINS, M. L. & NARUSE, M. (1980). *Brighton EMAG* 1979 *Conf. Proceedings.* London: Inst. of Physics.

FLOWERS, H. M., TIGHE, N. & SWANN, P. (1974). *High-Voltage Electron Microscopy, Proc. 3rd Internat. Conf.* London: Academic Press.

FROST, R. F. (1979). Unpublished.

GAI, P. L. (1980). III Climax Int. Conf. on Mo Chemistry, Ann Arbor, USA.

LINDSLEY, D. H., (1976). *Oxide Minerals*, edited by D. RUMBLE. *Mineral. Soc. Am. Short Course Notes*, Vol. III.

SMITH, G. H. & BURGE, R. E. (1962). *Acta Cryst.* **15**, 182–186.

SMITH, P. P. K. (1978). *Philos. Mag.* **B38**, 99–102.

SWANN, P. & TIGHE, N. (1971). *Jernkontorets Ann.* **155**, 497–500.

THOENI, W., GAI, P. L. & HIRSCH, P. B. (1977). *J. Less Common Met.* **54**, 263–271.

Acta Cryst. (1980). A**36**, 682–686

Absorption and Extinction Corrections: Standard Tests

BY H. D. FLACK AND M. G. VINCENT*

Laboratoire de Cristallographie aux Rayons X, Université de Genève, 24, quai Ernest Ansermet, CH 1211 Genève 4, Switzerland

AND N. W. ALCOCK

Department of Chemistry and Molecular Sciences, University of Warwick, Coventry CV4 7AL, England

(*Received* 11 *January* 1980; *accepted* 18 *February* 1980)

Abstract

The standard-test tables of values of transmission factors and $\bar{T}$, the absorption-weighted mean path lengths, given by Cahen & Ibers [*J. Appl. Cryst.* (1972), **5**, 298–299; *J. Appl. Cryst.* (1973), **6**, 244] and Alcock [*Acta Cryst.* (1974), A**30**, 332–335] have been corrected and extended.

Introduction

A difficult problem in producing a computer program is that of making sure that it is thoroughly tested. We

* Present address: Biozentrum der Universität Basel, Klingelbergstrasse 70, CH 4056 Basel, Switzerland.

0567-7394/80/040682-05$01.00